

Energy release rate of the fiber/matrix interface crack growth in $[0_{m \cdot 2n}^{\circ}, 90_n^{\circ}]_S$ laminates under transverse loading: effect of $0^{\circ}/90^{\circ}$ interface

Luca Di Stasio^{a,b}, Janis Varna^b, Zoubir Ayadi^a

^a Université de Lorraine, EEIGM, IJL, 6 Rue Bastien Lepage, F-54010 Nancy, France

^b Luleå University of Technology, University Campus, SE-97187 Luleå, Sweden

Abstract

Models of Representative Volume Elements (RVEs) of cross-ply $[0_{m \cdot 2n}^{\circ}, 90_n^{\circ}]_S$ laminates with different geometric configurations and damage states are studied. Debond growth is characterized by the estimation of the Mode I and Mode II Energy Release Rate (ERR) using the Virtual Crack Closure Technique (VCCT) and the J-integral. It is found that the presence of the $0^{\circ}/90^{\circ}$ interface and the thickness of the 0° layer have no effect, apart from laminates with *ultra-thin* 90° plies where it is however modest. With the exception of cross-ply laminates with an *ultra-thin* 90° ply, no difference is found in debond ERR between a UD composite and a cross-ply laminate.

Keywords: Polymer-matrix Composites (PMCs), Thin-ply, Transverse Failure, Debonding, Finite Element Analysis (FEA)

1. Introduction

Since the development of the *spread tow* technology or “FUKUI method” [1, 2], significant efforts have been directed toward the characterization of *thin-ply* laminates [3, 4, 5, 6, 7, 8, 9, 10, 11, 12, 13, 14, 15] and their application to mission-critical structures in the aerospace sector [16, 17, 18, 19].

At the lamina level, the use of *thin-ply*s leads to more regular and homogeneous microstructures [9, 12]. Measurement of ply level properties (tensile and compressive modulus, Poisson’s ratio, ultimate tensile strength, tensile on-

set of damage, interlaminar shear strength) on UD specimens ($[0_m^\circ]$ and $[90_m^\circ]$)
10 revealed no remarkable difference with average properties available in the literature for the same type of fiber, nor showed any particular dependence on the ply thickness [12]. Only an increase of the ultimate compressive strength in the fiber direction was observed with very thin plies (~ 4 fiber diameters), although with very scattered values, which the authors claim to be due to the
15 fiber arrangement's increased regularity which prevents the onset of fiber microbuckling [12]. A number of researchers [4, 5, 6, 7] has reported improvements in fatigue life with the use of *thin-ply*s, which are explained as a consequence of delayed propagation of free edge delaminations and intralaminar cracks. Several researchers have in fact analyzed the beneficial effect of *thin-ply*s on damage
20 development under static [3, 6, 7, 8, 9, 10, 11, 12], fatigue [4, 6, 7, 8, 12] and impact loadings [6, 7, 8, 12]. It seems apparent that *thin-ply* laminates possess an increased ability to delay, and in some cases even suppress, the onset and propagation of intralaminar cracks (or transverse or matrix or micro-cracks).
The first appearance of transverse cracks is known to be characterized by the
25 occurrence of fiber/matrix interface cracks (also referred to as debonds), which grow along the fiber arc direction, then kink out of the interface and coalesce forming a transverse crack [20]. Different approaches have been applied to model the initiation and growth of debonds. The Cohesive Zone Model (CZM) has been used to mimic the propagation of debonds along fiber interfaces; coupled with a failure criterion for the matrix, it has provided simulations of the
30 growth of transverse cracks starting from a virgin material [21, 22, 23, 24]. The main advantages of this approach are the possibility to observe the development of a simulated crack path and to record a load-displacement curve to compare with experimental measurement. However, various observations cast a doubt
35 about the applicability of the CZM: the bi- (for 2D models) and tri- (in 3D) axially of the matrix stress state in the inter-fiber region that is linked with a cavitation-like failure of the polymer [25]; the locality and mode dependency of the interface failure [26]; the problematic use at the microscopic level of properties measured in UD specimens at the laminate level [22]. A second approach

40 that obviates these drawbacks is the application of Linear Elastic Fracture Me-
 chanics (LEFM) arguments to the study of debond growth. The analysis focuses
 on the evaluation of Mode I and Mode II Energy Release Rate (ERR) at the
 crack tip by means of the Virtual Crack Closure Technique (VCCT) [27] or the
 J-Integral method [28]. The stress and strain field, required for the ERR compu-
 45 tation, can be solved by application of different methodologies such as analytical
 solutions [29], the Boundary Element Method (BEM) [30] or the Finite Element
 Method (FEM) [31]. The limitation of this approach is that it describes prop-
 agation of the debond, not its initiation. Finite fracture mechanics [32] is one
 way how to address the initiation problem. Different works have followed the
 50 LEFM approach and studied models of one or two fibers in an effectively infinite
 matrix [33, 34, 35, 36, 37] and of an hexagonal cluster of fibers in an effectively
 infinite homogenized UD composite [38, 31]. The problem of debond growth
 along the fiber-matrix interface in a cross-ply laminate has been only addressed
 very recently in [39, 40], where authors embed a single partially debonded fiber
 55 in an effectively infinite homogenized 90° ply bounded by homogenized 0° lay-
 ers. Thus, the effect of debond-debond interaction and of the relative proximity
 of a $0^\circ/90^\circ$ interface on the debond's ERR in cross-ply laminates is yet to be
 addressed. The present work is devoted to this problem. Models of Repeating
 Unit Cells (RUCs) are developed to represent laminates with different degrees
 60 of damage (here only in the form of debonds). The number of fully bonded
 fibers across the thickness of the 90° ply is varied in order to investigate the
 effect of the proximity of the $0^\circ/90^\circ$ interface. The thickness of the bounding 0°
 layers is also used as a parameter of the study. The stress and strain fields are
 solved with the Finite Element Method in Abaqus [41] and the debond (crack)
 65 is characterized by its Mode I and Mode II ERR, calculated with the VCCT
 and the J-integral method.

2. RVE models & FE discretization

2.1. Introduction & Nomenclature

In the present work, we investigate debond development under in-plane
70 transverse tension in $[0_{m \cdot 2n}^\circ, 90_n^\circ]_S$ laminates, where $2n$ is the thickness of the
central 90° layer expressed in terms of the number n of plies constituting it and
 $m \cdot 2n$ represents the thickness of the 0° layer as a multiple of the 90° layer
thickness. The interaction between debonds in the presence of an interface with
a stiff layer is studied with the use of different Repeating Unit Cells (RUCs)
75 (see Figures 1 and 2 in Sec. 2.2), in which only the central fiber is partially
debonded. Repetition of the composite RUC can occur only along the in-plane
transverse direction, thus representing a cross-ply laminate with a thin or even
ultra-thin 90° ply in the middle.

The thickness of the 90° ply depends on the number of fibers present across the
80 thickness (the vertical or z direction in Figures 1 and 2) and the value of the
fiber volume fraction V_f . On the other hand, the thickness of the 0° layers can
be assigned freely as a multiple of the 90° ply thickness, i.e. $t_{0^\circ} = i \cdot t_{90^\circ}$ where
 i is an arbitrary integer. The thickness ratio i could in theory be assumed to be
a real positive number; however, it seems more reasonable to consider it only
85 as a positive integer based on practical considerations on the actual manufac-
turing of laminates (stacking of a discrete number of pre-impregnated layers).
Thus, the thickness ratio i represents one additional parameter for the investiga-
tion. In the RUCs proposed, we consider the 90° ply with debonds as a series of
stacked damaged and undamaged fiber rows, each row with only one fiber in the
90 thickness direction. All the RUCs present regular microstructures with fibers
placed according to a square-packing configuration and consequently they are
Representative Volume Elements (RVE) of cross-ply laminates with a certain
distribution of debonds in the middle 90° layer. In the following, let us consider
in-plane coordinates x and y , where x is in the transverse direction of the cross-
95 ply laminate under consideration. In the presence of a load in the x -direction,
the strain in the y -direction is small, due to the very small minor Poisson's ratio

of the laminate. Furthermore, debonds are considered to be significantly longer in the fiber direction than in the arc direction [42]. Therefore we use 2D models under the assumption of plane strain, defined in the $x - z$ section of the composite. The study presented in this paper thus applies to long debonds and its focus is on understanding the mechanisms of growth along their arc direction. The laminates are assumed to be subject to transverse tensile strain, which is applied in the form of a constant displacement in the x -direction along both vertical boundaries of the RUC as shown in Figure 3.

In summary, the models are differentiated by: first, the spacing between debonds along the horizontal direction in the 90° layer, which corresponds to the number n of fibers in the RUC's horizontal direction; second, the thickness of the middle 90° ply measured in terms of the number k of fiber rows; third, the factor i which provides the thickness of the 0° layers as an integer multiple of the 90° ply thickness. It thus seems natural to introduce the common notation $n \times k - i \cdot t_{90^\circ}$. A final additional model is considered to study the effect of equivalent boundary conditions. This final model is constituted by only one partially debonded fiber. The application of coupling of horizontal displacements in the form of a constant applied displacement along the right and left sides allows for repetition along the horizontal direction. The presence of coupling of vertical displacements and a linear distribution of horizontal displacements on the bottom and top surfaces models the presence of the stiff $0^\circ/90^\circ$ interface between the 90° and the 0° layers. This model is referred to as $1 \times 1 - H + V$ given that: it has respectively 1 fiber in the horizontal and in the vertical direction; on the top and bottom surfaces, both horizontal (H) and vertical (V) displacements are assigned. Finally, two single fiber models similar to $1 \times 1 - H + V$ are considered in the present work for comparison: the $1 \times 1 - free$ and $1 \times 1 - coupling$. In the first, the upper surface is left free; in the second, vertical displacement coupling is applied to the upper boundary. Further details about these models and the corresponding laminate RVE can be found in [43].

2.2. Models of Representative Volume Element (RVE)

The first family of models is represented in Figure 1. It represents a set of $[0_{m \cdot 2n}^{\circ}, 90_n^{\circ}]_S$ cross-ply laminates with an ultra-thin 90° layer, constituted by a single row of fibers across the thickness. Debonds appear at regular intervals measured in terms of number n of fully bonded fibers present between them, which in turn correspond to the number of fibers along the horizontal direction of the RUC as highlighted in Fig. 1. They are thus the $n \times 1 - i \cdot t_{90^{\circ}}$ models, where $i = 1, 10$ and n is an integer ≥ 1 ($n = 1$ corresponds to the case of a debond appearing on all the fibers in the central 90° layer). These models are quite extreme, but allow to focus on the interaction between debonds and the inter-ply $0^{\circ}/90^{\circ}$ interface. Furthermore, the *spread tow* technology is today capable of producing cross-ply laminates with the central 90° layer thickness only 4 – 5 times the fiber diameter, as shown for example in [9], which give practical relevance even to such extreme models.

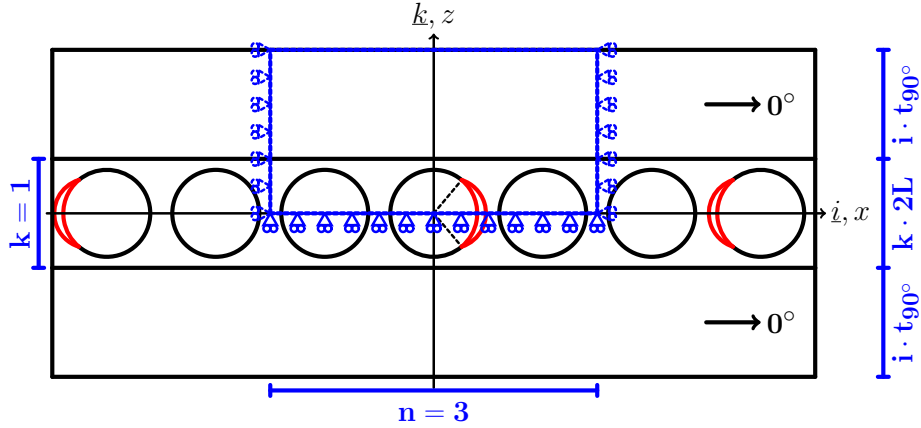


Figure 1: Models of $[0_{m \cdot 2n}^{\circ}, 90_n^{\circ}]_S$ cross-ply laminates with an ultra-thin 90° layer, where the 90° ply is made up by a single “row” of fibers. Debonds are repeating at different distances, measured in terms of the number n of fully bonded fibers appearing between two consecutive debonds.

The second set of models considers instead cross-ply laminates with a central 90° ply of variable thickness, measured in terms of number k of fiber rows appearing in the vertical direction in Figure 2. Once again, debonds appear at

regular intervals measured in terms of number n of fully bonded fibers present between them, which in turn correspond to the number of fibers along the horizontal direction of the RUC as highlighted in Fig. 2. These models are thus
145 the $n \times k - i \cdot t_{90^\circ}$ models, where $i = 1, 10$, $k > 1$ and n is an integer ≥ 1 ($n = 1$ corresponds to the case of a debond appearing on all the fibers of the central fiber row in the 90° layer).

By increasing the number n of fibers in the horizontal direction in the RUC,
150 decreasing levels of damage (debonds spaced further apart) are considered to be present in the laminate. By increasing the number k of fiber rows, the thickness of the 90° layer is increased and the effect of the relative proximity of the interply $0^\circ/90^\circ$ interface can thus be studied. Finally, by increasing the factor i , the thickness of the 0° layers is increased for a given thickness of the 90° , which
155 allows the investigation of the size effect or *in-situ* effect for the fiber-matrix interface crack.

2.3. Finite Element (FE) discretization

The RUCs are discretized using the Finite Element Method (FEM) with the commercial FEM package Abaqus [41]. The length l and height h of the
160 model are determined by the number of fibers n in the horizontal direction, the number of fiber rows k across the thickness and the thickness ratio i (see Sec. 2.2) according to Eq. 1:

$$l = 2nL \quad h = (1 + 2i)kL. \quad (1)$$

In Eq. 1, $2L$ is the length of a one-fiber unit (see Fig. 3), which in turn is as a function of the fiber volume fraction V_f and the fiber radius according to

$$L = \frac{R_f}{2} \sqrt{\frac{\pi}{V_f}}. \quad (2)$$

165 Each fiber in the model has the same radius R_f , equal to $1 \mu m$. This specific value has no physical meaning per se and it has been selected for simplicity. It is useful to observe that, in a linear elastic solution as the one described in the

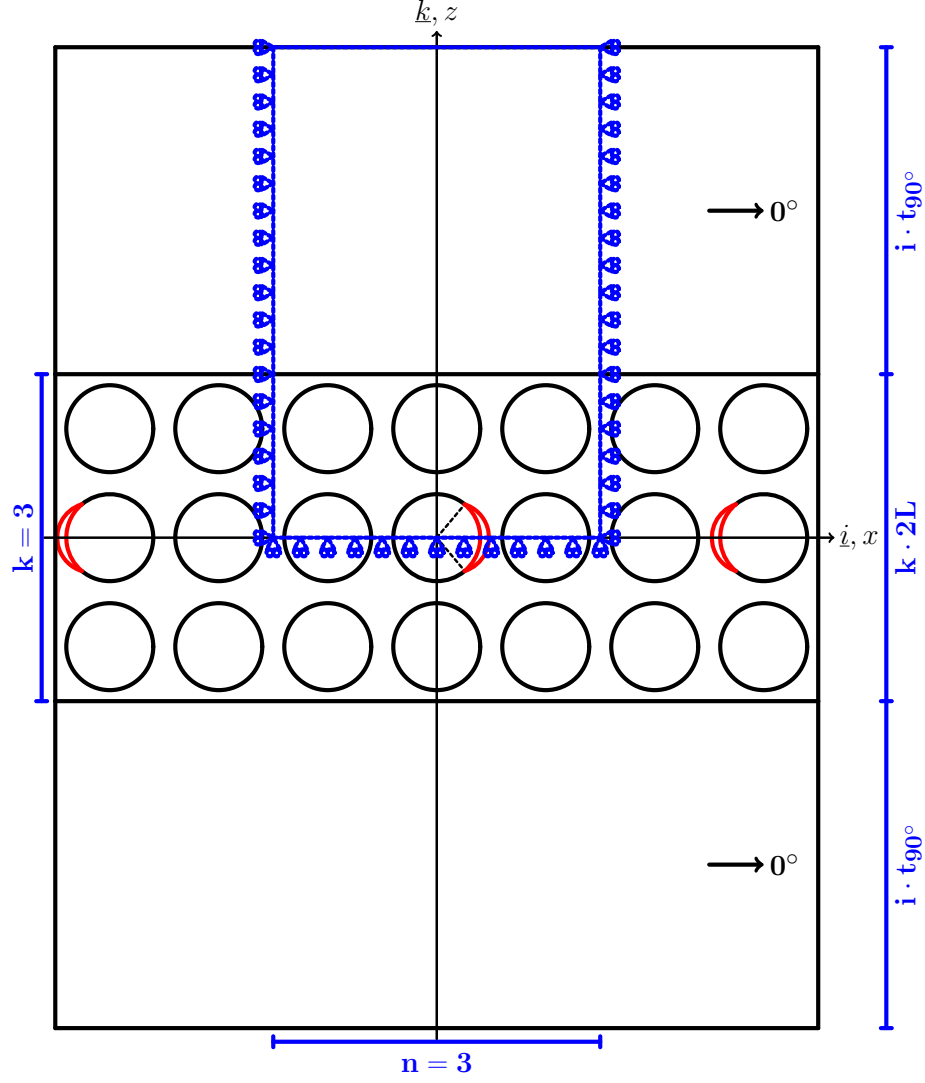


Figure 2: Models of $[0_{m \cdot 2n}^{\circ}, 90_n^{\circ}]_S$ cross-ply laminates with a 90° layer of variable thickness, determined by the number k of “rows” of fibers along the vertical direction. Debonds are repeating at different distances along the horizontal direction, measured in terms of the number n of fully bonded fibers appearing between two consecutive debonds.

present article, the ERR is proportional to the geometrical dimensions of the model and thus re-evaluation of the ERR for fibers of any size requires just
170 a multiplication. Furthermore, the local and global V_f are everywhere equal

thanks to the relationships in Eqs. 1 and 2.

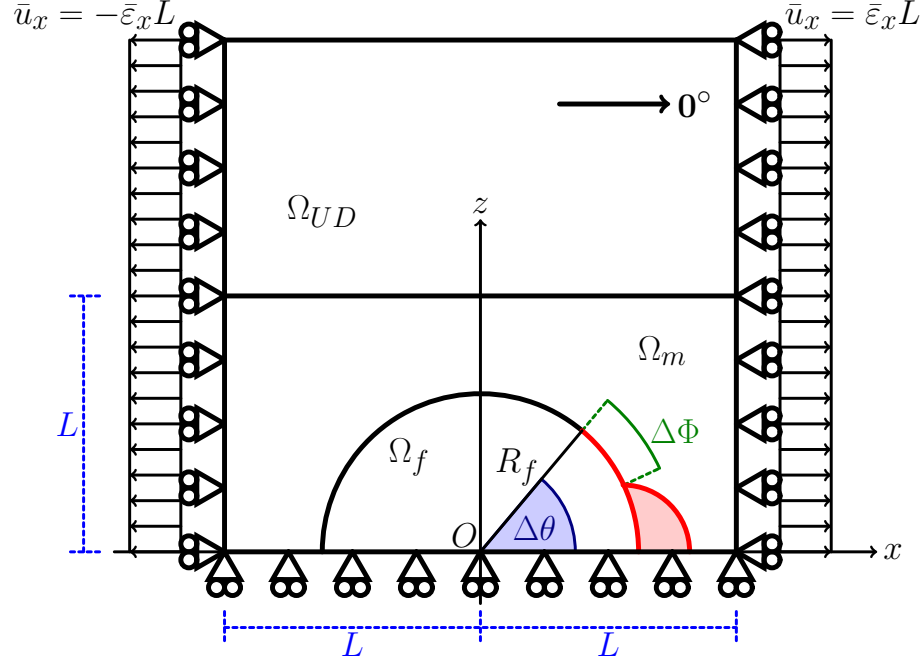


Figure 3: Schematic of the model with its main parameters.

The debond appears symmetrically with respect to the x axis (see Fig. 3) and we characterize it with the angular size $\Delta\theta$ (the full debond size is thus $2\Delta\theta$). In the case of large debond sizes ($\geq 60^\circ - 80^\circ$), a region of size $\Delta\Phi$ to be
175 determined by the solution itself appears at the crack tip. In this region, called the *contact zone*, the crack faces are in contact and slide on each other. Due to existence of the contact zone, frictionless contact is considered between the two crack faces to avoid interpenetration and allow free sliding. Symmetry with respect to the x axis is applied on the lower boundary. The upper boundary
180 is free, except for the model $1 \times 1 - H + V$ which requires on the upper side kinematic coupling of vertical displacements and applied linearly distributed horizontal displacements. Kinematic coupling on the x -displacement is applied along the left and right boundaries of the model in the form of a constant x -displacement $\pm\bar{\epsilon}_x l$, corresponding to transverse strain $\bar{\epsilon}_x$ equal to 1%.

Table 1: Summary of the mechanical properties of fiber, matrix and UD layer. E stands for Young’s modulus, μ for shear modulus and ν for Poisson’s ratio. Indexes L and T stand respectively for *longitudinal* and *transverse*.

Material	V_f [%]	E_L [GPa]	E_T [GPa]	μ_{LT} [GPa]	ν_{LT} [–]	ν_{TT} [–]
Glass fiber	-	70.0	70.0	29.2	0.2	0.2
Epoxy	-	3.5	3.5	1.25	0.4	0.4
UD	60.0	43.442	13.714	4.315	0.273	0.465

185 The FEM model is discretized using second order, 2D, plane strain triangular (CPE6) and rectangular (CPE8) elements. In the crack tip neighborhood, a refined regular mesh of quadrilateral elements with almost unitary aspect ratio is needed to ensure a correct evaluation of the ERR. The angular size δ of an element in this refined region close to the crack tip is by design equal to 0.05° .

190 The crack faces are modeled as element-based surfaces with a frictionless small-sliding contact pair interaction. The Mode I, Mode II and total Energy Release Rates (ERRs) (respectively G_I , G_{II} and G_{TOT}) represent the main result of the numerical analysis. They are computed using the VCCT [27] implemented in a custom Python routine and the total ERR is obtained from the J-integral [28]

195 evaluation by means of the Abaqus built-in functionality. Glass fiber and epoxy are considered throughout this article, and it is assumed that their response always lies in the linear elastic domain. The effective UD properties are computed using Hashin’s Concentric Cylinder Assembly model [44] with the self-consistency scheme for the out-of-plane shear modulus of Christensen [45]. The

200 properties used are listed in Table 1. The model was validated with respect to BEM results of [46, 36]; considerations about the order of accuracy can be found in [43].

3. Results & Discussion

3.1. Effect of the proximity of the $0^\circ/90^\circ$ $0^\circ/90^\circ$ interface and of the thickness of the 0° layer on debond ERR

We first focus our attention on the model $1 \times 1 - i \cdot t_{90^\circ}$, which represents a particular case of the family $n \times 1 - i \cdot t_{90^\circ}$. It corresponds to a cross-ply laminate in which the central 90° ply is constituted by only one fiber row, in which each fiber possesses a debond appearing on alternating sides. The model thus represents an extreme idealization, in the sense that: the central 90° layer is the thinnest that can be conceived and cannot actually be produced; second, a very particular damage state is present for which every fiber is partially debonded from the surrounding matrix. However, the first condition allows us to investigate the direct effect of the proximity of the stiff $0^\circ/90^\circ$ $0^\circ/90^\circ$ interface on debond ERR; the second condition prevents the insurgence of strain magnification effects which would be significant in one-fiber-row ply with debonds appearing at regular intervals of fully bonded fibers [43]. The model $1 \times 1 - i \cdot t_{90^\circ}$ thus isolates the effect of the $0^\circ/90^\circ$ $0^\circ/90^\circ$ interface. Given that the ratio $i = \frac{t_{0^\circ}}{t_{90^\circ}}$ is a free parameter, we can furthermore study the effect of the thickness of the 0° layer on debond ERR.

In Figures 4 and 5 respectively the Mode I and Mode II ERR are compared between models $1 \times 1 - i \cdot t_{90^\circ}$ with $i = 1, 10, 50, 100$ and models $1 \times 1 - free$, $1 \times 1 - coupling$ and $1 \times 1 - H + V$. It is worth to remind us of the laminate RVE that correspond to these last three models: model $1 \times 1 - free$ represents a one-fiber-row UD composite with all the fibers partially debonded; model $1 \times 1 - coupling$ corresponds to a UD laminate with an infinite number of fiber rows and all the fibers partially debonded; model $1 \times 1 - H + V$ represents a cross-ply laminate with one-fiber-row central 90° ply. Observing Figure 4, it is possible to notice that the presence of the $0^\circ/90^\circ$ $0^\circ/90^\circ$ interface translates into a modest increase in the value of G_I with respect to the free surface. For every value of the thickness, however, the values of G_I are lower than those computed with the $1 \times 1 - coupling$ and $1 \times 1 - H + V$ models. A more significant effect can

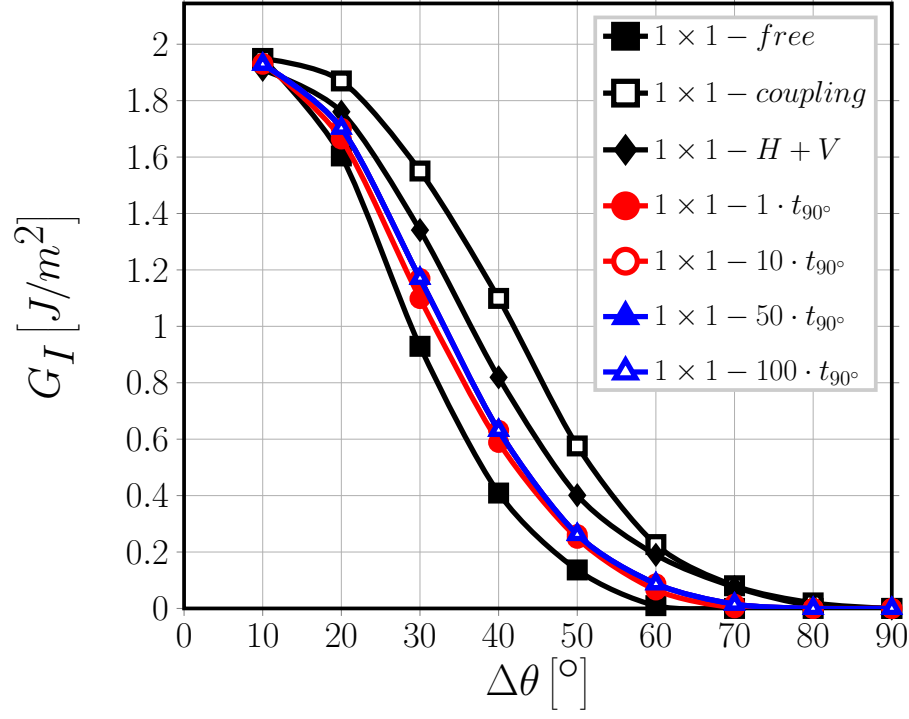


Figure 4: Effect of the proximity of the $0^\circ/90^\circ$ $0^\circ/90^\circ$ interface and of the thickness of the 0° layer on Mode I ERR: models $1 \times 1 - free$, $1 \times 1 - coupling$, $1 \times 1 - H + V$ and $1 \times 1 - i \cdot t_{90^\circ}$. $V_f = 60\%$, $\varepsilon_x = 1\%$.

be observed in relation to contact zone onset, which is delayed from $\Delta\theta = 60^\circ$ in the presence of a free surface to 70° in the presence of a homogenized 0° layer. The maximum delay is however reached with the models with equivalent
235 boundary conditions ($1 \times 1 - coupling$ and $1 \times 1 - H + V$), for which the contact zone onset happens at $\Delta\theta = 80^\circ$. No effect of the thickness of the 0° layer on Mode I ERR can be observed.

The presence of the $0^\circ/90^\circ$ $0^\circ/90^\circ$ interface causes instead a decrease of
240 Mode II for open debonds ($\Delta\theta < 60^\circ - 70^\circ$) and a decrease for close debonds ($\Delta\theta > 60^\circ - 70^\circ$) with respect to the free surface case (see Fig. 5). The trend is the same as the one of the model $1 \times 1 - H + V$, but more modest in magnitude. A small effect of the thickness of the 0° layer on Mode II ERR can be noticed



Figure 5: Effect of the proximity of the $0^\circ/90^\circ$ $0^\circ/90^\circ$ interface and of the thickness of the 0° layer on Mode II ERR: models $1 \times 1 - free$, $1 \times 1 - coupling$, $1 \times 1 - H + V$ and $1 \times 1 - i \cdot t_{90^\circ}$. $V_f = 60\%$, $\varepsilon_x = 1\%$.

in Fig. 5 when the ratio $i = \frac{t_{0^\circ}}{t_{90^\circ}}$ is increased from 1 to 10. The change between
245 the two follows the same pattern described previously: when the thickness of
the 0° ply is increased, Mode II decreases for open debonds and increases for
closed debonds.

These results help to shed light on the effect of the $0^\circ/90^\circ$ $0^\circ/90^\circ$ interface
on debond ERR. The presence of the stiff homogenized 0° layer causes the
250 matrix placed relatively far from the fiber (close to the left and right sides) to
contract much less than it would do in the presence of a free surface due to its
relatively high Poisson's ratio. Furthermore, the presence of the $0^\circ/90^\circ$ $0^\circ/90^\circ$
interface induces a more homogeneous x -displacement field all over the matrix
domain. This causes a concurrent increase of G_I and decrease of G_{II} for small

255 debonds, where the crack opening displacement component at the crack tip
 (responsible for Mode I) is mostly due to the global x -displacement field (which
 increase in the presence of the $0^\circ/90^\circ$ $0^\circ/90^\circ$ interface) while the crack shear
 displacement component at the crack tip (responsible for Mode II) is instead
 linked to the global vertical displacement field due to Poisson's effect (which is
 260 decreasing). This causes also the delay in the onset of the contact zone. For
 large debonds instead, after the onset of the contact zone, the situation reverses:
 the magnitude increase of the global x -displacement field leads to an increase in
 the crack shear displacement component at the crack tip and thus in Mode II
 ERR. By comparing the results for Mode II of models $1 \times 1 - free$, $1 \times 1 - H + V$
 265 and $1 \times 1 - i \cdot t_{90^\circ}$ with $i = 1, 10, 50, 100$ (Fig. 5), it can be argued that the effect
 of the 0° ply thickness is related to the distance of the free surface: for $t_{0^\circ} = t_{90^\circ}$
 a modest effect of the presence of the upper free surface of the 0° ply is still felt
 by the debond and the effect of the $0^\circ/90^\circ$ $0^\circ/90^\circ$ interface previously described
 is reduced, with the ERR values closer to the $1 \times 1 - free$ model. When the
 270 thickness ratio is increased to 10, the effect disappears. No further change is
 observed for thicker 0° layers.

3.2. *Effect of the proximity of the $0^\circ/90^\circ$ $0^\circ/90^\circ$ interface on debond-debond interaction in a single fiber row 90° ply*

We turn now our attention to the models $n \times 1 - 1 \cdot t_{90^\circ}$, which correspond to
 275 a cross-ply laminate in which the central 90° ply is constituted by only one fiber
 row where debonds appear on alternating sides of the damaged fiber at regular
 intervals of $n - 1$ fully bonded fibers (see Figure 1). This class of models allows
 to study the effect of the presence of the 0° layer on debond-debond interaction
 and, particularly, crack shielding [47, 43].

280 From Figures 6 and 7 it seems apparent that the effect of the presence of the
 $0^\circ/90^\circ$ $0^\circ/90^\circ$ interface is to reduce the x -strain magnification caused by the
 presence of an increasing number of fully bonded fibers between two consecutive
 debonds. Effects observed in the previous section (Sec. 3.1) are also retrievable
 in Figures 6 and 7. For Mode I, irrespectively of the number of undamaged

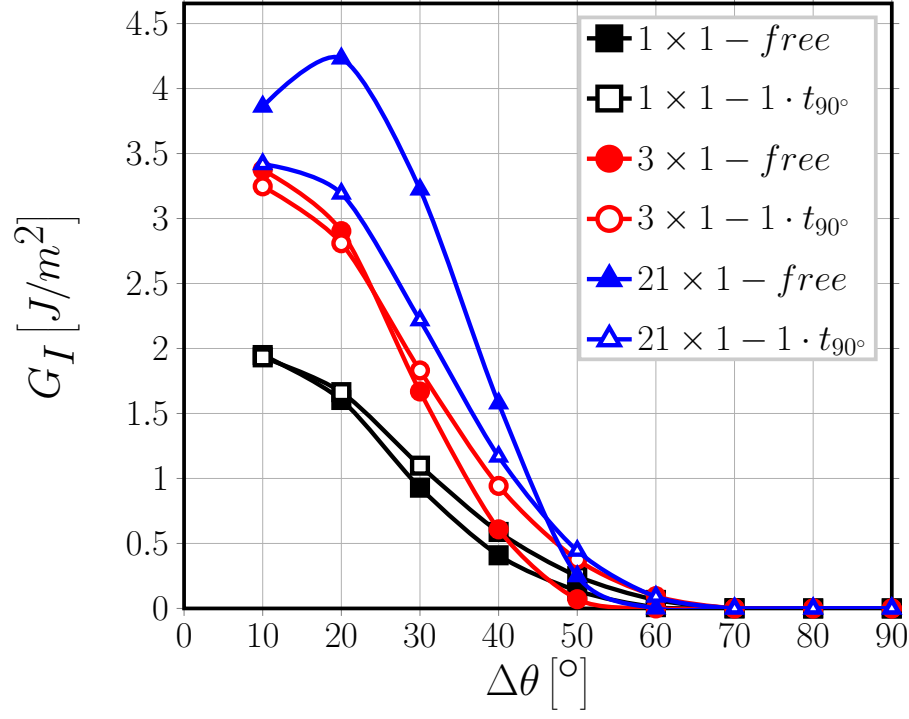


Figure 6: Effect of the presence of the 0° layer on debond-debond interaction for Mode I ERR: models $n \times 1 - free$ and $n \times 1 - 1 \cdot t_{90^\circ}$. $V_f = 60\%$, $\varepsilon_x = 1\%$.

fibers between two consecutive debonds, the contact zone onset is shifted by $\sim 10^\circ$ from 60° in the presence of a free surface to 70° when the $0^\circ/90^\circ$ $0^\circ/90^\circ$ interface is present. For Mode II it is possible to observe, especially when debonds are closer to each other, that larger debonds show a slightly higher G_{II} , as discussed in Sec. 3.1.

3.3. Effect of the presence of fiber rows with no damage on the debond- $0^\circ/90^\circ$ $0^\circ/90^\circ$ interface interaction

After having investigated the effect of the proximity of the $0^\circ/90^\circ$ $0^\circ/90^\circ$ interface and of the thickness of the 0° layer on debond ERR and on debond-debond interaction, we address in this section the effect of the presence of fiber rows with only fully bonded fibers inside (and thus no damage) on the interaction between debonds and the $0^\circ/90^\circ$ $0^\circ/90^\circ$ interface interaction. To this end, we

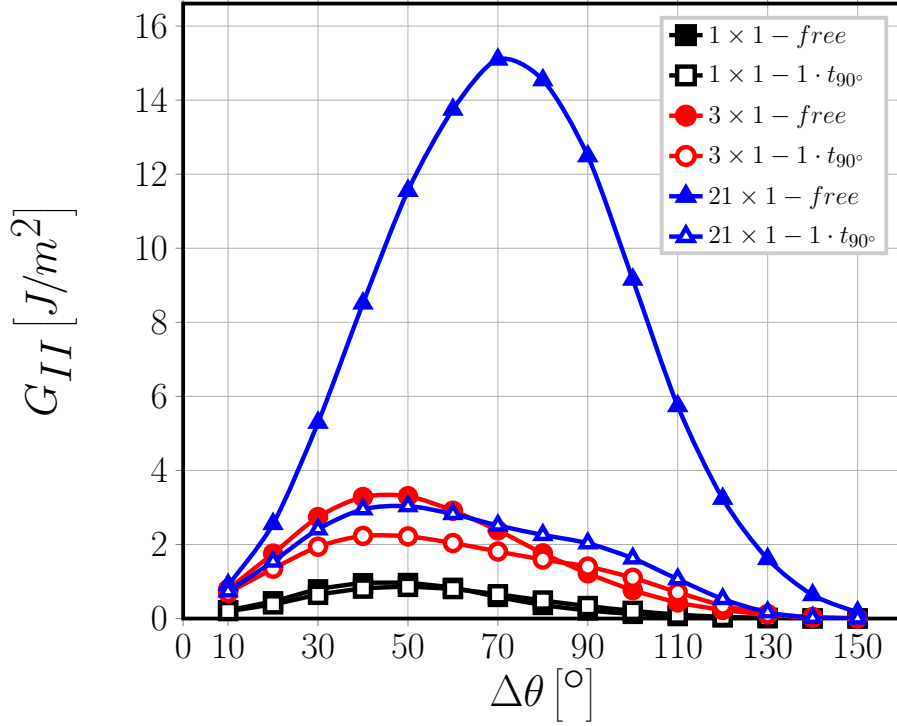


Figure 7: Effect of the presence of the 0° layer on debond-debond interaction for Mode II ERR: models $n \times 1 - free$ and $n \times 1 - 1 \cdot t_{90^\circ}$. $V_f = 60\%$, $\varepsilon_x = 1\%$.

study the models $1 \times k - 1 \cdot t_{90^\circ}$, which represent a cross-ply laminate with the central 90° ply made of k fiber rows and where all the fibers in the central row are partially debonded. Given that today 90° layers with around 4 – 5 fibers across the thickness are manufacturable thanks to the *thin-ply* technology, this family of models considers a quite realistic geometric configuration of the 90° ply, although ideally organized following a perfect square-packing arrangement. The damage state represents on the other hand quite an extreme idealization: however, the fact that all the fibers in the central row are partially debonded prevents the presence of strain magnification effects.

Figures 8 and 9 show clearly that the presence of the 0° ply does not affect in any measurable way the debond ERR neither in Mode I nor in Mode II: there is no difference in G_I G_{II} between models $1 \times k - free$ and $1 \times k - 1 \cdot t_{90^\circ}$.

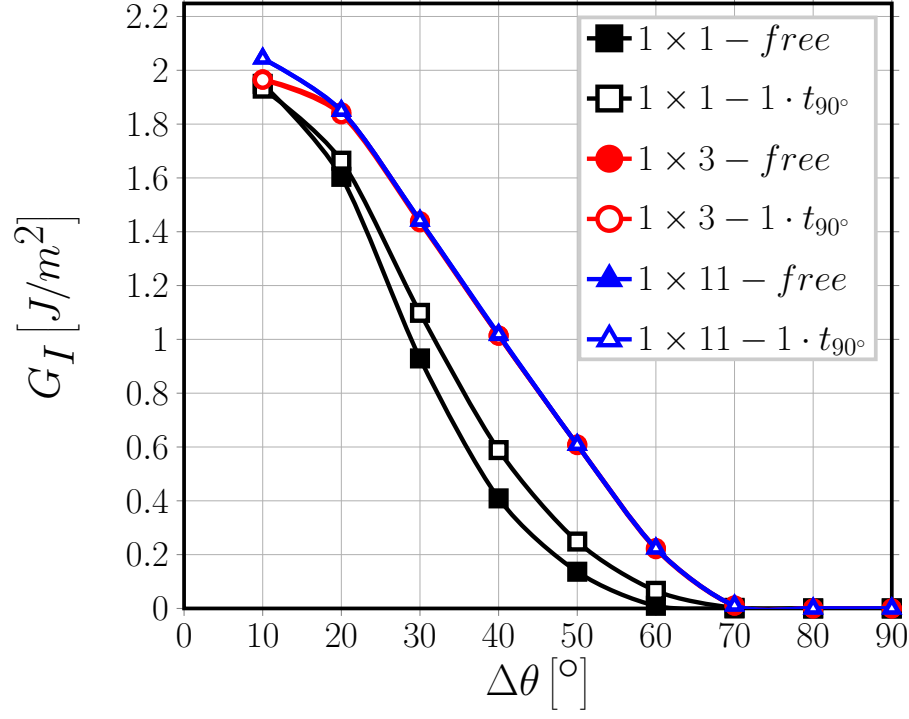


Figure 8: Effect of the presence of undamaged fiber rows in the 90° layer on debond- $0^\circ/90^\circ$ $0^\circ/90^\circ$ interface interaction for Mode I ERR: models $1 \times k - free$ and $1 \times k - 1 \cdot t_{90^\circ}$. $V_f = 60\%$, $\varepsilon_x = 1\%$.

However, in Figures 8 and 9 the central fiber row of the 90° layer possesses
 310 only partially debonded fibers, which represents an extreme damage state. It
 has been shown that the presence of fully bonded fibers causes a magnification of
 the x -strain in the debond neighborhood which leads to an increase in ERR both
 in one-fiber-row UD [43] and 90° ply in cross-ply laminates (Sec. 3.2). When
 rows of undamaged fibers are present above and below the fiber row containing
 315 the debonds, the presence of the $0^\circ/90^\circ$ $0^\circ/90^\circ$ interface has, with respect to
 the free surface case (corresponding to an extremely thin UD composite), no
 effect on G_I and only a small effect on G_{II} , relevant only for thin 90° plies
 (see Figures 10 and 11). When present, this effect corresponds to a reduction
 in Mode II ERR, particularly for debonds further apart (in terms of number of



Figure 9: Effect of the presence of undamaged fiber rows in the 90° layer on debond- $0^\circ/90^\circ$ $0^\circ/90^\circ$ interface interaction for Mode II ERR: models $1 \times k - free$ and $1 \times k - 1 \cdot t_{90^\circ}$. $V_f = 60\%$, $\varepsilon_x = 1\%$.

fully bonded fibers between them).

In [39, 40], the authors investigated the existence of scale effects (like the *thin-ply effect*) in the context of the fiber-matrix interface crack using a single partially debonded fiber embedded in a homogenized 90° ply bounded by homogenized 0° layers. They observed the absence of any size effect. The results presented in this article confirm their observation and provide a micromechanical explanation (see Sec. 3.1). We have also shown that extremely thin 90° plies (1 – 5 fibers across the thickness) do on the other hand present a magnification effect when fully bonded fibers appear between consecutive aligned debonds. The effect becomes stronger with thinner 90° layers. The only effect of the 0° ply is to reduce the magnification of ERR, which nonetheless takes



Figure 10: Effect of the presence of undamaged fiber rows in the 90° layer on debond- $0^\circ/90^\circ$ $0^\circ/90^\circ$ interface interaction for Mode I ERR: models $n \times k - free$ and $n \times k - 1 \cdot t_{90^\circ}$. $V_f = 60\%$, $\varepsilon_x = 1\%$.

place. However, this mechanism is not typical of cross-ply laminates, but it can be observed in UD composites as well [43]. It provides a possible mechanical description of the observations presented in [9]: in very thin 90° plies debonds appear at lower strains because the magnification effect is stronger. As more debonds are created, their interaction (crack shielding) causes a reduction in ERR which disfavors debond growth.

4. Conclusions & Outlook

Different models of Repeating Unit Cell, representing different representative cross-ply laminates, have been studied in order to study the effect of the presence of the $0^\circ/90^\circ$ $0^\circ/90^\circ$ interface and of the thickness of the 0° ply on debond



Figure 11: Effect of the presence of undamaged fiber rows in the 90° layer on debond- $0^\circ/90^\circ$ $0^\circ/90^\circ$ interface interaction for Mode II ERR: models $n \times k - free$ and $n \times k - 1 \cdot t_{90^\circ}$. $V_f = 60\%$, $\varepsilon_x = 1\%$.

Energy Release Rate and on crack shielding. It has been found that the presence of the 0° ply causes only a reduction in ERR, especially in Mode II. However, the strain magnification effect due to the presence of fully bonded fibers between two consecutive debonds follows the same pattern previously identified for UD
 345 composites. Furthermore, the influence of the 0° layer is strongly mitigated by the presence of rows of undamaged fibers. Already the presence of 1 row between respectively the upper and lower 0° layer and the central fiber row with partially debonded fibers causes the computed Mode I and Mode II ERR to adhere closely to the results for a UD composite with the same geometrical configuration and
 350 damage state. The results presented provide an important insight: it appears that the behavior of the fiber/matrix interface crack is affected strongly only by

very close perturbation of the elastic fields. *Thin* and *ultra-thin* plies present a peculiar behavior in terms of debond growth because their reduced thickness brings the $0^\circ/90^\circ$ $0^\circ/90^\circ$ interface close enough for the debonds to feel the perturbation in the elastic fields. Otherwise, it seems that no difference can be found in the mechanism of debond growth between a UD composite and a cross-ply laminate.

Acknowledgements

Luca Di Stasio gratefully acknowledges the support of the European School of Materials (EUSMAT) through the DocMASE Doctoral Programme and the European Commission through the Erasmus Mundus Programme.

References

- [1] K. Kawabe, New spreading technology for carbon fiber tow and its application to composite materials, *Sen'i Gakkaishi* 64 (8) (2008) 262–267. doi:10.2115/fiber.64.p_262.
- [2] K. Kawabe, H. Sasayama, S. Tomoda, New carbon fiber tow-spread technology and applications to advanced composite materials, *SAMPE Journal* 45 (2) (2008) 6–17.
- [3] H. Sasayama, K. Kawabe, S. Tomoda, I. Ohsawa, K. Kageyama, N. Ogata, Effect of lamina thickness on first ply failure in multidirectionally laminated composites, in: *Proceedings of the 8th Japan SAMPE Symposium*, SAMPE, 2003.
- [4] K. Yamaguchi, H. Hahn, The improved ply cracking resistance of thin-ply laminates, in: *Proceedings of the 15th International Conference on Composite Materials (ICCM-15)*, SAMPE, 2005.
- [5] S. Tsai, S. Sihm, R. Kim, Thin ply composites, in: *Proceedings of 46th AIAA/ASME/AHS/ASC Structures, Structural Dynamics & Materials Conference*, 2005.

- [6] S. Sihh, R. Kim, K. Kawabe, S. Tsai, Experimental studies of thin-ply laminated composites, *Composites Science and Technology* 67 (6) (2007) 996–1008. doi:10.1016/j.compscitech.2006.06.008.
- [7] T. Yokozeki, Y. Aoki, T. Ogasawara, Experimental characterization of strength and damage resistance properties of thin-ply carbon fiber/toughened epoxy laminates, *Composite Structures* 82 (3) (2008) 382–389. doi:10.1016/j.compstruct.2007.01.015.
- [8] T. Yokozeki, A. Kuroda, A. Yoshimura, T. Ogasawara, T. Aoki, Damage characterization in thin-ply composite laminates under out-of-plane transverse loadings, *Composite Structures* 93 (1) (2010) 49–57. doi:10.1016/j.compstruct.2010.06.016.
- [9] H. Saito, H. Takeuchi, I. Kimpara, Experimental evaluation of the damage growth restraining in 90 layer of thin-ply cfrp cross-ply laminates, *Advanced Composite Materials* 21 (1) (2012) 57–66. doi:10.1163/156855112X629522.
- [10] A. Arteiro, G. Catalanotti, J. Xavier, P. Camanho, Notched response of non-crimp fabric thin-ply laminates, *Composites Science and Technology* 79 (2013) 97–114. doi:10.1016/j.compscitech.2013.02.001.
- [11] A. Arteiro, G. Catalanotti, J. Xavier, P. Camanho, Large damage capability of non-crimp fabric thin-ply laminates, *Composites Part A: Applied Science and Manufacturing* 63 (2014) 110–122. doi:10.1016/j.compositesa.2014.04.002.
- [12] R. Amacher, J. Cugnoni, J. Botsis, L. Sorensen, W. Smith, C. Dransfeld, Thin ply composites: Experimental characterization and modeling of size-effects, *Composites Science and Technology* 101 (2014) 121–132. doi:10.1016/j.compscitech.2014.06.027.
- [13] G. Guillaumet, A. Turon, J. Costa, J. Renart, P. Linde, J. Mayugo, Damage occurrence at edges of non-crimp-fabric thin-ply laminates under off-axis

uniaxial loading, *Composites Science and Technology* 98 (2014) 44–50. doi:10.1016/j.compscitech.2014.04.014.

- 410 [14] C. Huang, S. Ju, M. He, Q. Zheng, Y. He, J. Xiao, J. Zhang, D. Jiang, Identification of failure modes of composite thin-ply laminates containing circular hole under tension by acoustic emission signals, *Composite Structures* 206 (2018) 70–79. doi:10.1016/j.compstruct.2018.08.019.
- 415 [15] J. Cugnoni, R. Amacher, S. Kohler, J. Brunner, E. Kramer, C. Dransfeld, W. Smith, K. Scobbie, L. Sorensen, J. Botsis, Towards aerospace grade thin-ply composites: Effect of ply thickness, fibre, matrix and interlayer toughening on strength and damage tolerance, *Composites Science and Technology* 168 (2018) 467–477. doi:10.1016/j.compscitech.2018.08.037.
- 420 [16] J.-B. Moon, M.-G. Kim, C.-G. Kim, S. Bhowmik, Improvement of tensile properties of CFRP composites under LEO space environment by applying MWNTs and thin-ply, *Composites Part A: Applied Science and Manufacturing* 42 (6) (2011) 694–701. doi:10.1016/j.compositesa.2011.02.011.
- 425 [17] Y. H. N. Kim, S. Ko, W.-S. Lay, J. Tian, P. Chang, S. U. Thielk, H.-J. Bang, J. Yang, Effects of shallow biangle, thin-ply laminates on structural performance of composite wings, *AIAA Journal* 55 (6) (2017) 2086–2092. doi:10.2514/1.j055465.
- [18] A. Kopp, S. Stappert, D. Mattsson, K. Olofsson, E. Marklund, G. Kurth, E. Mooij, E. Roorda, The aurora space launcher concept, *CEAS Space Journal* 10 (2) (2017) 167–187. doi:10.1007/s12567-017-0184-2.
- 430 [19] D. A. McCarville, J. C. Guzman, A. K. Dillon, J. R. Jackson, J. O. Birkland, 3.5 Design, Manufacture and Test of Cryotank Components, Elsevier, 2018, pp. 153–179. doi:10.1016/b978-0-12-803581-8.09958-6.
- [20] J. E. Bailey, A. Parvizi, On fibre debonding effects and the mechanism of transverse-ply failure in cross-ply laminates of glass fibre/thermoset

- 435 composites, *Journal of Materials Science* 16 (3) (1981) 649–659. doi:
10.1007/bf02402782.
- [21] V. Kushch, S. Shmegeera, P. Brøndsted, L. Mishnaevsky, Numerical simulation of progressive debonding in fiber reinforced composite under transverse loading, *International Journal of Engineering Science* 49 (1) (2011) 17–29.
440 doi:10.1016/j.ijengsci.2010.06.020.
- [22] L. P. Canal, C. González, J. Segurado, J. LLorca, Intraply fracture of fiber-reinforced composites: Microscopic mechanisms and modeling, *Composites Science and Technology* 72 (11) (2012) 1223–1232. doi:10.1016/j.compscitech.2012.04.008.
- 445 [23] L. Bouhala, A. Makradi, S. Belouettar, H. Kiefer-Kamal, P. Frères, Modelling of failure in long fibres reinforced composites by x-FEM and cohesive zone model, *Composites Part B: Engineering* 55 (2013) 352–361. doi:10.1016/j.compositesb.2012.12.013.
- [24] M. Herráez, D. Mora, F. Naya, C. S. Lopes, C. González, J. LLorca,
450 Transverse cracking of cross-ply laminates: A computational micromechanics perspective, *Composites Science and Technology* 110 (2015) 196–204. doi:10.1016/j.compscitech.2015.02.008.
- [25] L. E. Asp, L. A. Berglund, P. Gudmundson, Effects of a composite-like stress state on the fracture of epoxies, *Composites Science and Technology*
455 53 (1) (1995) 27–37. doi:10.1016/0266-3538(94)00075-1.
- [26] V. Mantič, Interface crack onset at a circular cylindrical inclusion under a remote transverse tension. application of a coupled stress and energy criterion, *International Journal of Solids and Structures* 46 (6) (2009) 1287–1304. doi:10.1016/j.ijsolstr.2008.10.036.
- 460 [27] R. Krueger, Virtual crack closure technique: History, approach, and applications, *Applied Mechanics Reviews* 57 (2) (2004) 109. doi:10.1115/1.1595677.

- [28] J. R. Rice, A path independent integral and the approximate analysis of strain concentration by notches and cracks, *Journal of Applied Mechanics* 35 (2) (1968) 379. doi:10.1115/1.3601206.
- [29] M. Toya, A crack along the interface of a circular inclusion embedded in an infinite solid, *Journal of the Mechanics and Physics of Solids* 22 (5) (1974) 325–348. doi:10.1016/0022-5096(74)90002-7.
- [30] F. París, J. C. Caño, J. Varna, The fiber-matrix interface crack — a numerical analysis using boundary elements, *International Journal of Fracture* 82 (1) (1996) 11–29. doi:10.1007/bf00017861.
- [31] L. Zhuang, A. Pupurs, J. Varna, R. Talreja, Z. Ayadi, Effects of inter-fiber spacing on fiber-matrix debond crack growth in unidirectional composites under transverse loading, *Composites Part A: Applied Science and Manufacturing* 109 (2018) 463–471. doi:10.1016/j.compositesa.2018.03.031.
- [32] M. Muñoz-Reja, L. Távara, V. Mantič, P. Cornetti, Crack onset and propagation at fibre-matrix elastic interfaces under biaxial loading using finite fracture mechanics, *Composites Part A: Applied Science and Manufacturing* 82 (2016) 267–278. doi:10.1016/j.compositesa.2015.09.023.
- [33] E. Correa, V. Mantič, F. París, Effect of thermal residual stresses on matrix failure under transverse tension at micromechanical level: A numerical and experimental analysis, *Composites Science and Technology* 71 (5) (2011) 622–629. doi:10.1016/j.compscitech.2010.12.027.
- [34] E. Correa, F. París, V. Mantič, Effect of the presence of a secondary transverse load on the inter-fibre failure under tension, *Engineering Fracture Mechanics* 103 (2013) 174–189. doi:10.1016/j.engfracmech.2013.02.026.
- [35] E. Correa, F. París, V. Mantič, Effect of a secondary transverse load on the inter-fibre failure under compression, *Composites Part B: Engineering* 65 (2014) 57–68. doi:10.1016/j.compositesb.2014.01.005.

- [36] C. Sandino, E. Correa, F. París, Numerical analysis of the influence of a nearby fibre on the interface crack growth in composites under transverse tensile load, *Engineering Fracture Mechanics* 168 (2016) 58–75. doi:10.1016/j.engfracmech.2016.01.022.
- 495 [37] C. Sandino, E. Correa, F. París, Interface crack growth under transverse compression: nearby fibre effect, in: *Proceeding of the 18th European Conference on Composite Materials (ECCM-18)*, 2018.
- [38] J. Varna, L. Q. Zhuang, A. Pupurs, Z. Ayadi, Growth and interaction of debonds in local clusters of fibers in unidirectional composites during transverse loading, *Key Engineering Materials* 754 (2017) 63–66. doi:10.4028/www.scientific.net/kem.754.63.
- 500 [39] M. Velasco, E. Graciani, L. Távara, E. Correa, F. París, BEM multiscale modelling involving micromechanical damage in fibrous composites, *Engineering Analysis with Boundary Elements* 93 (2018) 1–9. doi:10.1016/j.enganabound.2018.03.012.
- 505 [40] F. París, M. L. Velasco, E. Correa, Micromechanical study on the influence of scale effect in the first stage of damage in composites, *Composites Science and Technology* 160 (2018) 1–8. doi:10.1016/j.compscitech.2018.03.004.
- 510 [41] Simulia, Providence, RI, USA, ABAQUS/Standard User’s Manual, Version 6.12 (2012).
- [42] H. Zhang, M. Ericson, J. Varna, L. Berglund, Transverse single-fibre test for interfacial debonding in composites: 1. experimental observations, *Composites Part A: Applied Science and Manufacturing* 28 (4) (1997) 309–315. doi:10.1016/s1359-835x(96)00123-6.
- 515 [43] L. D. Stasio, J. Varna, Z. Ayadi, Energy release rate of the fiber/matrix interface crack in ud composites under transverse loading: debond-debond

and debond-free boundary interactions, submitted to Theoretical and Applied Fracture Mechanics.

- 520 [44] Z. Hashin, Analysis of composite materials—a survey, *Journal of Applied Mechanics* 50 (3) (1983) 481. doi:10.1115/1.3167081.
- [45] R. Christensen, K. Lo, Solutions for effective shear properties in three phase sphere and cylinder models, *Journal of the Mechanics and Physics of Solids* 27 (4) (1979) 315–330. doi:10.1016/0022-5096(79)90032-2.
- 525 [46] F. París, E. Correa, V. Mantič, Kinking of transversal interface cracks between fiber and matrix, *Journal of Applied Mechanics* 74 (4) (2007) 703. doi:10.1115/1.2711220.
- [47] I. García, V. Mantič, E. Graciani, Debonding at the fibre–matrix interface under remote transverse tension. one debond or two symmetric debonds?,
530 *European Journal of Mechanics - A/Solids* 53 (2015) 75–88. doi:10.1016/j.euromechsol.2015.02.007.